Axisymmetric turbulent wakes with new non-equilibrium similarity scalings

J. Nedić,[1,*] J. C. Vassilicos,[1,†] and B. Ganapathisubramani[2,‡]

[1] *Turbulence, Mixing and Flow Control Group, Department of Aeronautics, Imperial College London, London SW7 2AZ, United Kingdom*[§]

[2] *Aerodynamics and Flight Mechanics Research Group, University of Southampton, Southampton SO17 1BJ, United Kingdom*

(Dated: September 18, 2013)

The recently discovered non-equilibrium turbulence dissipation law implies the existence of axisymmetric turbulent wake regions where the mean flow velocity deficit decays as the inverse of the distance from the wake-generating body and the wake width grows as the square root of that distance. This behaviour is different from any documented boundary-free turbulent shear flow to date. Its existence is confirmed in wind tunnel experiments of wakes generated by plates with irregular edges placed normal to an incoming free stream. The wake characteristics of irregular bodies such as buildings, bridges, mountains, trees, coral reefs and wind turbines are critical in many areas of environmental engineering and fluid mechanics.

As described in many turbulence textbooks, mean turbulence spatial profiles (e.g. mean flow and turbulence intensity profiles) are self-similar/self-preserving in far enough regions of many boundary-free turbulent shear flows, such as various turbulent wakes, jets and plumes. Turbulent flows are also archetypal dissipative phenomena and another property central to their understanding and modelling is the dissipation rate ε of turbulence kinetic energy K at high Reynolds number (a number representing the ratio between inertial and viscous forces). Tennekes & Lumley [1] refer to the widely known and used high Reynolds number assumption $\varepsilon \sim K^{3/2}/L$ (where L is an appropriate correlation length-scale giving a measure of the large turbulent eddies) as "one of the cornerstone assumptions of turbulence theory". Other authors refer to this cornerstone assumption as the "zeroth law of turbulence" [2]. In particular, it is central to mean field theories of turbulent flows called Reynolds Averaged Navier-Stokes (RANS) models [3] and to coarse-graining approaches called Large Eddy Simulations (LES) [4]; and it is also an integral part of the Kolmogorov-Richardson phenomenology of turbulent spectral equilibrium [5] which has been a centrepiece in our understanding and modelling of small-scale turbulence since the 1940s (e.g. the estimate that the number of turbulent degrees of freedom is proportional to the $9/4$ power of Reynolds number relies on $\varepsilon \sim K^{3/2}/L$).

One important way in which the zeroth law is key is its pivotal role in determining the scaling laws of self-similar/self-preserving free shear turbulent flow profiles. As shown by George [6], these profiles are obtained from the average momentum equation (with neglected viscous force as the Reynolds number is high), the kinetic energy equation and an assumption on dissipation. These two equations determine the streamwise evolutions of the self-similar/self-preserving mean flow and kinetic energy profiles in the plane normal to the streamwise direction. Whilst the mean flow U is shaped by the turbulence via the turbulent (Reynolds) stress R, also assumed self-similar/self-preserving, the spatial dependence of the kinetic energy K is shaped by the effects of turbulent production $\mathcal{P}$, transport $\mathcal{T}$ and dissipation ε, all of which are assumed self-similar/self-preserving too. This procedure is not conclusive, however, without an assumption on the dissipation, and this is where the zeroth law is key [6].

Work over the past six years has revealed the existence of regions in the lee of both fractal and regular grids where a new high Reynolds number dissipation law holds [7–12], different from $\varepsilon = C_\varepsilon K^{3/2}/L$ with C_ε independent of Reynolds number. In these regions, $C_\varepsilon \sim Re_G^m/Re_L^n$ where n and m are both close to 1, Re_G is a global Reynolds number based on inlet/boundary conditions and Re_L is a local Reynolds number based on local velocity and length scales. Re_L decays with streamwise distance from the turbulence-generating grid in these regions which were termed non-equilibrium regions by [10] in the expectation that the rate of nonlinear energy transfer across length-scales does not balance dissipation as the new dissipation law strongly suggests a non-Richardson-Kolmogorov cascade [8].

In most boundary-free turbulent shear flows (plane wakes, mixing layers, jets and plumes) the local Reynolds number does not decrease with increasing streamwise distance from the source [1]. A notable exception of great engineering, environmental, geophysical and scientific importance is the axisymmetric turbulent wake [1]. As the non-equilibrium regions discovered to date are regions where the local Reynolds number decreases with distance from various types of grids, we make the assumption in this work that the non-equilibrium dissipation law may also exist in some regions of some axisymmetric wakes generated by objects which, like grids, combine wake-like with jet-like behaviours. Examples of such objects are the plates in figures 1(c), 1(d) and 1(e). We may expect such non-axisymmetric plates to have axisymmetric mean wakes far enough downstream as

any average non-axisymmetry will be erased by the accompanying non-axisymmetric turbulent (Reynolds) stresses [13].

Adopting cylindrical coordinates (x, r, φ) where x is the streamwise distance from the object causing the turbulent wake, r is the radial distance from the streamwise axis and φ is the azimuthal angle, and assuming axisymmetry (i.e. no dependence on φ), we can write the following self-similar/self-preservation functional forms in terms of a length-scale $\delta(x)$ which can be taken to be the wake's integral width: $U_\infty - U = u_0(x)f(\eta)$, where $f(0) = 1$ and $\eta = r/\delta$, and where U and U_∞ (the constant upstream flow velocity) are both in the streamwise direction; $R = R_0(x)g(\eta); K = K_0(x)h(\eta); \mathcal{T} = \mathcal{T}_0(x)\tau(\eta)$ and $\varepsilon = D_0(x)e(\eta)$. The wake's integral width is defined by $u_0\delta^2 = \int_0^\infty (U_\infty - U)rdr$. One can then introduce these forms into the average momentum and kinetic energy equations for the axisymmetric wake exactly as done in [6] (i.e. $U_\infty \frac{\partial}{\partial x}(U_\infty - U) = -\frac{1}{r}\frac{\partial}{\partial r}(rR)$ and $U_\infty \frac{\partial K}{\partial x} = -R\frac{\partial U}{\partial r} + \mathcal{T} - \varepsilon$) with the following resulting five solvability conditions: $d\delta/dx \sim R_0/(U_\infty u_0)$, $d\delta/dx \sim \mathcal{T}_0/(U_\infty K_0)$, $d\delta/dx \sim D_0\delta/(U_\infty K_0)$, $K_0 \sim u_0^2$ and $u_0\delta^2 \sim U_\infty\theta^2$ where θ is the momentum thickness defined by $\pi U_\infty^2\theta^2 = 2\pi\int_0^\infty U_\infty(U - U_\infty)rdr$ which is a constant independent of x (because of momentum balance) in the absence of a free-stream pressure gradient in the wind tunnel. As there are six variables involved in these five solvability conditions, an extra relation is required to close the system and obtain the scaling laws for the streamwise decay of the mean flow defect $u_0(x)$ and the streamwise growth of the local wake width $\delta(x)$. Whilst this extra relation is usually taken to be $D_0 \sim K_0^{3/2}/L \sim u_0^3/\delta$ in accordance with the usual "zeroth law", we take it to be $D_0 \sim (U_\infty\ell/\nu)^m(u_0\delta/\nu)^{-n}u_0^3/\delta$ where ℓ is the size of the bluff body generating the wake. The usual zeroth law is recovered when $n = m = 0$, and the new non-equilibrium dissipation law is recovered when n and m are both close to 1. The resulting scaling laws are (in terms of a virtual origin x_0 which comes out naturally from the analysis):

$$u_0(x)/U_\infty \sim \left(\frac{x - x_0}{\theta}\right)^{-\frac{2}{3-n}} Re_G^{\frac{2(n-m)}{3-n}} (\ell/\theta)^{-\frac{2n}{3-n}} \quad (1)$$

$$\delta(x)/\theta \sim \left(\frac{x - x_0}{\theta}\right)^{\frac{1}{3-n}} Re_G^{\frac{m-n}{3-n}} (\ell/\theta)^{\frac{n}{3-n}} \quad (2)$$

where the global Reynolds number $Re_G \equiv (U_\infty\ell)/\nu$. For $n = m = 0$ one recovers the well-known scalings $u_0(x)/U_\infty \sim \left(\frac{x-x_0}{\theta}\right)^{-\frac{2}{3}}$ and $\delta(x)/\theta \sim \left(\frac{x-x_0}{\theta}\right)^{\frac{1}{3}}$, which can be found in textbooks such as Townsend [13] and Tennekes & Lumley [1]. For $n = m = 1$ the new prediction based on the assumption that non-equilibrium regions may exist in axisymmetric turbulent wakes is that

$$u_0(x)/U_\infty \sim \left(\frac{x - x_0}{\theta}\right)^{-1} (\theta/\ell) \quad (3)$$

and

$$\delta(x)/\theta \sim \left(\frac{x - x_0}{\theta}\right)^{1/2} (\ell/\theta)^{1/2} \quad (4)$$

in such regions. Both these scalings are valid in the fully turbulent regime and the coefficients multiplying them are independent of Reynolds number Re_G. The new scalings should not be confused with the low Reynolds number scalings $u_0(x)/U_\infty \sim Re_G(\frac{x-x_0}{\theta})^{-1}(\theta/\ell)$ and $\delta(x)/\theta \sim Re_G^{-1/2}(\frac{x-x_0}{\theta})^{1/2}(\ell/\theta)^{1/2}$ of [6] obtained by setting $m = 0$ and $n = 1$. These are low Reynolds number scalings because they result from the low Reynolds number dissipation form $D_0 \sim \nu u_0^2/\delta^2$ which is not valid in fully developed turbulent shear flows. They differ from the new scalings by their dependence on Re_G.

Studies of axisymmetric wakes go back more than sixty years and the bluff bodies which were used as wake generators are mostly spheres and disks placed normal to the incoming stream [14–17]. The new scaling laws (3) and (4) suggest significantly more rate of mixing of momentum than usual and we must therefore chose wake generators accordingly. Nedić et al [18] showed that the plates in figures 1(c),1(d) and 1(e) generate significantly more drag than disks (figure 1(a)), square plates (figure 1(b)) and many other plates of equal surface area when placed normal to a free stream. For this reason and because they combine wake-like with jet-like behaviours, we use the high-drag plates in figures 1(c),1(d) and 1(e) to demonstrate the existence of scaling laws (3) and (4), our first task being to establish that, far enough from the plates, the wakes are statistically axisymmetric.

Two sets of the five flat plates shown in figure 1 were used to generate turbulent wakes. The frontal area $\mathcal{A}$ of the plates is the same in each set thus defining one same size $\ell \equiv \sqrt{\mathcal{A}}$. However, $\ell = 64mm$ with thickness 1.25mm in one set whereas $\ell = 128mm$ with thickness 2.5mm in the other, thus doubling the Reynolds number Re_G from one set to the other without changing U_∞ which was kept at 10m/s in all our experiments. Each plate was suspended in the centre of the wind tunnel normal to the laminar free stream and 0.5m from the start of the working section using four 0.2mm diameter piano wires. The wind tunnel has a closed recirculating loop with a 9:1 contraction ratio, a working cross-section of 0.91m x 0.91m and a working length of 4.25m. The background turbulence level at the freestream velocity $U_\infty = 10m/s$ is 0.05%. Hot wire anemometry measurements were taken downstream of the wake generators using a Dantec Dynamics 55P51 X-wire, driven by a Dantec StreamLine CTA system. The wires were 5μm in diameter, 3mm

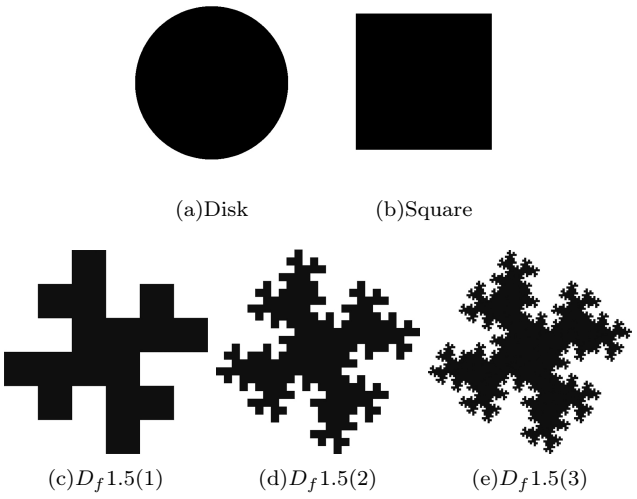

FIG. 1. Drawings of (a) a disk, (b) a square plate and three high-drag plates with irregular edges. The self-similar process leading from (b) to (c) to (d) to (e) leads, if continued ad infinitum, to a plate with a fractal perimeter of infinite length and fractal dimension D_f = 1.5 but same surface area. All drawings are to scale so that the areas of the disk and all the plates are the same. For the $\ell = 64mm$ set of plates, the normalised perimeter P/ℓ and the momentum thickness θ are (a) $2\sqrt{\pi}$, 19.08mm; (b) 4, 18.91mm; (c) 8, 20.69mm; (d) 16, 20.89mm; (e) 32, 20.87mm.

long Pt-W wire with a sensing length of 1.25mm and connected to a 55H24 6mm probe holder.

To obtain mean turbulent wake profiles, the probe was traversed at each one of the positions x/ℓ = 5, 10, 15, 20, 25, 30, 35, 40, 45, 50 in 15mm horizontal intervals normal to the streamwise x-axis, covering a distance of 390mm from the centre-line. For the smaller plates with $\ell = 64mm$ at the two closest distances x/ℓ = 5 and 10, the X-wire was traversed in 10mm steps up to a distance of 260mm from the centre-line as these particular wake widths were considerably smaller and more data points were required to get good spatial resolution. Data was sampled using a 16-bit National Instruments NI-6229 (USB) data acquisition card, at a rate of 20kHz for 30 seconds, which was sufficient to obtain converged statistics of the mean and fluctuating velocities for both velocity components.

To ascertain the statistical axisymmetry of our wakes we investigated the azimuthal variations of the mean and fluctuating flow profiles. These variations were obtained by rotating the plate and taking measurements at various azimuthal angles, in particular φ = 0°, 15°, 30° ... 90°. In table I we list the coefficients of variance with φ of various wake statistics. The conclusion is that the wake statistics are indeed axisymmetric to a good approximation at $x/\ell \geq 10$ and increasingly so for increasing x/ℓ. At $x = 10\ell$ there is already less than 2% variation in all statistics

TABLE I. Given a data set $\mathcal{S}(r,\phi)$ where $\mathcal{S}$ stands for mean flow profile U/U_∞, turbulence intensity profiles $\frac{<u_x'^2>^{0.5}}{U_\infty}$ and $\frac{<u_r'^2>^{0.5}}{U_\infty}$ or Reynolds stress profile $\frac{<u_x'u_r'>}{U_\infty^2}$, the coefficient of variance is $c_v(r) \equiv 100\sqrt{\frac{1}{N_\varphi}\sum_\varphi(\mathcal{S}(r,\varphi)-\overline{\mathcal{S}}(r))^2}/\overline{\mathcal{S}}(r)$ where $\overline{\mathcal{S}}(r) \equiv \frac{1}{N_\varphi}\sum_\varphi \mathcal{S}(r,\varphi)$ and N_φ is the number of different azimuthal measurements. This table lists values of the average and maximum (in brackets) coefficients of variance $\overline{c_v} \equiv \frac{1}{N_r}\sum_r c_v(r)$ and $c_v^{max} \equiv \max_r c_v(r)$ where N_r is the number of radial data points. Note that these coefficients of variance are given as percentages.

Plate	x/ℓ	$\frac{U}{U_\infty}$	$\frac{<u_x'^2>^{0.5}}{U_\infty}$	$\frac{<u_r'^2>^{0.5}}{U_\infty}$	$\frac{<u_x'u_r'>}{U_\infty^2}$
Disk	10	0.38 (0.53)	1.47 (2.38)	1.26 (2.29)	4.63 (8.31)
Square	10	0.27 (0.57)	1.38 (2.83)	1.65 (3.66)	5.76 (13.10)
1.5(2)	10	0.47 (0.66)	1.88 (4.59)	1.56 (3.72)	4.55 (9.55)
1.5(2)	20	0.27 (0.45)	1.57 (5.62)	1.65 (3.25)	4.19 (8.42)
1.5(2)	30	0.16 (0.33)	1.37 (3.32)	1.10 (2.85)	4.11 (6.98)

for all plates, with only the Reynolds stress showing a variation of less than 6% (see table I). Finally, it is also worth mentioning that we verified the constancy of θ with x and that $u_0\delta^2 \sim U_\infty\theta^2$.

The self-similarity/self-preservation of the streamwise mean flow profiles and the Reynolds stresses was thoroughly tested for all our wake-generators and found to hold for $x \geq 15\ell$. Some of the results demonstrating this self-similarity are plotted in figure 2. On the basis of the mean flow profiles we can calculate the wake integral width $\delta(x)$ and the centreline velocity deficit $u_0(x)$. In figure 3 we plot $(\delta(x)/\theta)^2$ and $(u_0(x)/U_\infty)^{-1}$ as functions of x/θ for all three high-drag plates in figures 1(c),1(d) and 1(e). In agreement with predictions (3) and (4), our data demonstrate clear well-defined linear relationships between $(\delta(x)/\theta)^2$ and x/θ and between $(u_0(x)/U_\infty)^{-1}$ and x/θ for all three high-drag plates over the streamwise range sampled. We also checked that the disk and square return wakes with the expected well-known linear dependencies of $(u_0(x)/U_\infty)^{-3/2}$ and $(\delta(x)/\theta)^3$ on x/θ [1, 13].

In Table II we report the best fit values for the coefficients A and B, the exponents α and β and the virtual origins in $u_0/U_\infty = A(\frac{x-x_0}{\theta})^{-\alpha}$ and $\delta/\theta = B(\frac{x-x_0}{\theta})^{\beta}$ for all plates in figure 1. Our fitting method is immune to the usual virtual origin problem and in fact returns actual values for these origins as explained in the caption of Table II. The fits are for 10 data points over the range x/ℓ = 5 to x/ℓ = 50 for all plates. Note how the values of α and β are close to 2/3 and 1/3 respectively for the disk and square, in agreement with classical studies of axisymmetric wakes behind regular objects. Note also how very close these exponents are, respectively, to the new scaling values 1 and 1/2 predicted by (3) and (4) for

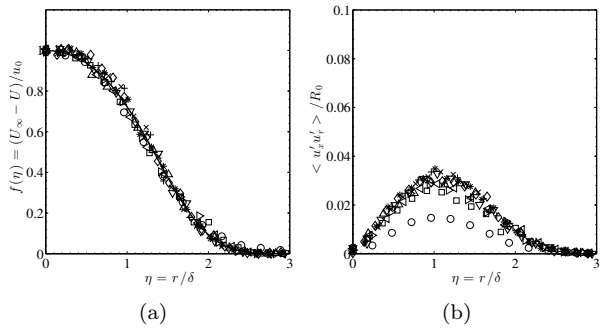

(a) (b)

FIG. 2. Mean flow and Reynolds stress profiles at different streamwise distances collapsed using similarity scalings for the $\ell = 64mm$, $D_f1.5(2)$ high-drag plate for downstream distances of $(\bigcirc) - 5\ell$; $(\square) - 10\ell$; $(\triangleright) - 15\ell$; $(\triangleleft) - 20\ell$; $(\triangle) - 25\ell$; $(\triangledown) - 30\ell$; $(+) - 35\ell$; $(\times) - 40\ell$; $(\star) - 45\ell$; $(\diamond) - 50\ell$. Note that $R_0 = u_0 U_\infty (d\delta/dx)$ here.

TABLE II. Best fits to $u_0/U_\infty = A(\frac{x-x_0}{\theta})^{-\alpha}$ and $\delta/\theta = B(\frac{x-x_0}{\theta})^{\beta}$ obtained by, first, calculating $\frac{d}{dx}(u_0/U_\infty)^{-1/\alpha}$ and $\frac{d}{dx}(\delta/\theta)^{1/\beta}$ for a range of values of α and β and estimating their respective linear fits $C_1 x/\theta + A^{-1/\alpha}$ and $C_2 x/\theta + B^{1/\beta}$, then choosing α and β such that $C_1 = C_2 = 0$ and deriving corresponding estimates for $A^{-1/\alpha}$ and $B^{1/\beta}$. Having A, α, B and β, we then obtain the virtual origin. In the table we list the values of the virtual origins x_{0A} and x_{0B} obtained independently for u_0/U_∞ and δ/θ respectively.

Plate	A	$-x_{0A}/\theta$	α	B	$-x_{0B}/\theta$	β
Disk	0.78	-12.78	0.68	1.14	-12.88	0.34
Square	0.47	-20.23	0.59	1.46	-20.34	0.29
1.5(1)	7.67	13.65	1.03	0.36	13.56	0.52
1.5(2)	6.53	12.13	1.01	0.39	11.96	0.51
1.5(3)	3.61	2.62	0.89	0.53	2.53	0.44

the irregular plates of figures 1(c,d) and closer to the new scalings than the classical ones for the irregular plate of figure 1(e). Of particular note is the fact that the virtual origins obtained independently from the wake deficit and the wake width data are very close to each other, as should indeed be the case.

At equal Re_G and frontal area $\mathcal{A}$, the local Reynolds number $u_0\delta/\nu$ of the high-drag plates (figures 1(c),1(d) and 1(e)) is about 50% higher than for the square and the disk (see figure 4(a)). This agrees with the higher values of A by factors between 4.6 and 16.3 and the lower values of B by factors between 2.1 and 4 for the high-drag plates compared to the regular ones (see Table II), consistent with the increase in drag. When doubling Re_G by going from $\ell = 64mm$ to $\ell = 128mm$ no significant changes were recorded in the values of $\delta(x)/\theta$ and $u_0(x)/U_\infty$. We are therefore clearly far from the low-Reynolds number regime obtained by setting $m = 0$ and $n = 1$ [6]. The similarity scalings which we observe are all high Reynolds

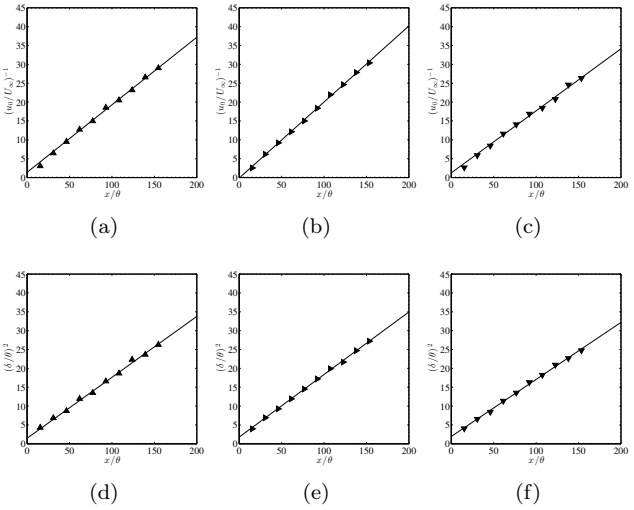

(a) (b) (c)

(d) (e) (f)

FIG. 3. $(u_0/U_\infty)^{-1}$ versus x/θ (top a, b, c plots) and $(\delta/\theta)^2$ versus x/θ (bottom d, e, f plots) for $\ell = 64mm$ high-drag plates. Left plots, $D_f1.5(1)$; centre plots, $D_f1.5(2)$; right plots, $D_f1.5(3)$.

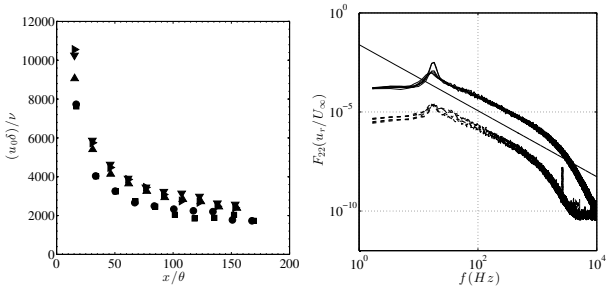

(a) (b)

FIG. 4. (a) Local Reynolds number $(u_0\delta/\nu)$ versus x/θ for disk - $(\bullet)$, square - $(\blacksquare)$, $D_f = 1.5(1)$ - $(\blacktriangle)$, $D_f = 1.5(2)$ - $(\blacktriangleright)$, $D_f = 1.5(3)$ - $(\blacktriangledown)$. (b) Energy spectra of radial velocity component for all $\ell = 64mm$ plates on the centre-line; solid lines at $x = 5\ell$ and dashed lines at $x = 50\ell$

number scalings. In fact, the energy spectra are broad and continuous with power-law regions which extend over one to two decades both at $x = 5\ell$ and at $x = 50\ell$ and for all plates including the disk and the square - figure 4(b).

We have presented a very extensive set of hot wire anemometry measurements which demonstrate the existence of axisymmetric wakes with the new non-equilibrium similarity scalings (3) and (4). These scalings imply that the local Reynolds number $u_0\delta/\nu$ decreases while the "memory", i.e. the ratio of the eddy turnover time δ/u_0 to the advection time x/U_∞, increases with x, unlike any documented free shear flow [19]. High-drag wake-generators resembling aspects of those of figures 1(c),1(d) and 1(e) can be expected to prevail in the natural and the built environments, e.g. bridges,

buildings and roof-tops, mountains, islands, trees, etc. Their wake properties may be much closer to those of our wakes than to any documented boundary-free turbulent shear flow.

We acknowledge EPSRC funding and thank Jacques Borée and W.K. George for helpful comments.

* jovan.nedic@imperial.ac.uk
† j.c.vassilicos@imperial.ac.uk
‡ g.bharath@soton.ac.uk
§ www.imperial.ac.uk/tmfc

[1] H. Tennekes and J. L. Lumley, *A first course in turbulence* (MIT press, 1972).
[2] B. Rollin, Y. Dubief, and C. R. Doering, Journal of Fluid Mechanics **670**, 204 (3 2011), ISSN 0022-1120.
[3] B. E. Launder and D. B. Spalding, "Lectures in mathematical models of turbulence, 1972," .
[4] C. Meneveau and J. Katz, Annual Review of Fluid Mechanics **32**, 1 (2000).
[5] G. K. Batchelor, *The theory of homogeneous turbulence* (Cambridge University Press, 1953).
[6] W. K. George, Advances in Turbulence, 39(1989).
[7] R. E. Seoud and J. C. Vassilicos, Physics of fluids **19**, 105108 (2007).
[8] N. Mazellier and J. C. Vassilicos, Physics of Fluids **22**, 075101 (2010).
[9] P. C. Valente and J. C. Vassilicos, Journal of Fluid Mechanics **687**, 300 (11 2011), ISSN 0022-1120.
[10] P. C. Valente and J. C. Vassilicos, Physical Review Letters **108** (5 2012), ISSN 0031-9007, doi: \bibinfo{doi}{10.1103/PhysRevLett.108.214503}.
[11] R. Gomes-Fernandes, B. Ganapathisubramani, and J. C. Vassilicos, Journal of Fluid Mechanics **711**, 306 (11 2012), ISSN 0022-1120.
[12] S. Discetti, I. B. Ziskin, T. Astarita, and R. Adrian, Fluid Dynamics Research **45**, 061401 (2013).
[13] A. A. Townsend, *The structure of turbulent shear flow* (Cambridge University Press, 1956).
[14] R. Fail, J. A. Lawford, and R. C. W. Eyre, *Low speed experiments on the wake characteristics of flat plates normal to an airstream* (Ministry of Aviation, 1957).
[15] T. Carmody, Journal of Basic Engineering **86**, 869 (1964).
[16] W. Humphries and J. H. Vincent, Applied Scientific Research **32**, 649 (1976).
[17] P. W. Bearman, Journal of Fluid Mechanics **46**, 177 (1971), ISSN 0022-1120.
[18] J. Nedić, B. Ganapathisubramani, and J. C. Vassilicos, Fluid Dynamics Research **45**, 061406 (2013).
[19] J. C. R. Hunt, I. Eames, C. B. da Silva, and J. Westerweel, Philos Trans A Math Phys Eng Sci **369**, 811 (2 2011), ISSN 1364-503X.